Oxidative Addition of RX to Soluble and Polymer-Bound Molybdenum Carbonyl Complexes

Katja Heinze,*[a] Volker Jacob,[a] and Christian Feige[a]

Keywords: Allyl Ligands / Molybdenum / Polymer-bound complexes / Solid-phase synthesis

Oxidative addition of $PhSnCl_3$ or allyl halides to molybdenum tetracarbonyl complexes proceeds both in solution and on polymer matrices. The structures of the soluble Mo^{II} complexes have been determined by single-crystal X-ray diffraction in the solid state and by NMR and IR spectroscopy in solution. The identity and stability of the polymer-bound complexes have been elucidated by spectroscopic techniques directly on the solid support and by releasing the complexes from the support.

Introduction

Homogeneous organometallic catalysis has several advantages over heterogeneous catalysis as the activity and selectivity can be tuned by the choice of suitable ligands. On the other hand soluble catalysts are more difficult to separate and to handle than the technically well-established heterogeneous ones. A promising strategy to combine the advantages of both catalyst types is the immobilisation of active metal complexes on supports, which can be separated by filtration. However, many of the heterogeneous systems are very difficult to characterise and are not well understood. Improved characterisation should lead to better reproducibility, whereas understanding on a molecular level, if possible, can help to improve existing concepts and to develop new catalytic systems.[1] This is even more important as some stoichiometric and catalytic reactions performed on polymer matrices give different results from the reactions performed in a homogeneous phase.[2] A polymer matrix can confer higher stability to reactive intermediates,[3,4] can stabilise catalytically active species ("site isolation" effect [5−7]) and thus lead to higher activity, but can also reduce catalyst activity and influence catalyst selectivity,[8] even enantioselectivity.[9] Thus it is desirable to identify and control the species bound to the polymer support.

As part of our program to synthesise and characterise metal complexes bound to a solid support[10−12] we investigated the transformation of polymer-bound Mo^0 complexes to Mo^{II} complexes by oxidative addition of RX and elimination of carbon monoxide. The oxidative addition of RX to Mo^0 is one of the first steps in the synthesis of the precatalyst of the molybdenum(0)-catalysed allylic alkylation developed by Trost et al.[13−15] This catalytic reaction has become an important tool in asymmetric organic synthesis. Control of catalyst regioselectivity and enantioselectivity has been achieved by designing suitable ligands and using suitable metal catalyst precursors.[13−16] Microwave flash heating has been employed to improve catalyst activity and the immobilisation of the nucleophile on a solid support has been reported.[17] An allylpalladium phosphane complex has been anchored to a polystyrene/poly(ethylene glycol) graft copolymer and has been used for the palladium-catalysed allylic substitution.[18] An allylmolybdenum complex has been synthesised on a solid support and released from the solid phase for biolabelling purposes.[19]

The solid-phase reaction system employed here allows the synthesis of metal complexes on an insoluble polystyrene/divinyl benzene copolymer, the transformation of these complexes on the support and finally release of the product complexes from the support under mild conditions to prove their identity and integrity.[11,12]

Results and Discussion

The Solid-Phase Synthesis of 3a−6a via 3b−6b and Solution Synthesis of 3a−6a

For the solid-phase synthesis the bidentate Schiff-base ligand **1a** was attached to polystyrene/2% divinyl benzene by a silyl ether linker to yield the immobilised ligand **1b** (Scheme 1).[10−12] This silyl ether can be cleaved by fluoride ions under mild conditions compatible with metal complexes.[11,12]

[a] Anorganisch-Chemisches Institut der Universität Heidelberg
Im Neuenheimer Feld 270, 69120 Heidelberg, Germany
Fax.: (internat.) + 49-(0)6221-545707
E-mail: katja.heinze@urz.uni-heidelberg.de

Supporting information for this article is available on the WWW under http://www.eurjic.org or from the author.

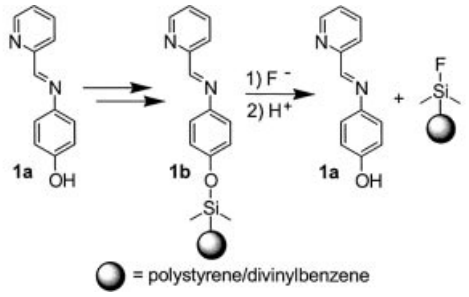

Scheme 1. Immobilisation of ligand **1a** and release of **1a** from the polymer

Solid-State Structures of 3a·Et_2O, 4a·THF, 5a·THF and 5a

The heterobimetallic complex **3a** crystallises in the monoclinic space group $P2_1/c$ with inclusion of one diethyl ether molecule (Figure 1, Table 1). The solvent molecule is attached to the complex by an O−H···O hydrogen bond (O1···O100 2.74 Å). Hydrogen bonds from the hydroxy group of the Schiff-base ligand to solvent molecules have been previously observed.[20] The molybdenum atom is seven-coordinate and the tin atom is five-coordinate with one chlorine atom occupying a bridging position between the two metal atoms. The coordination geometry around

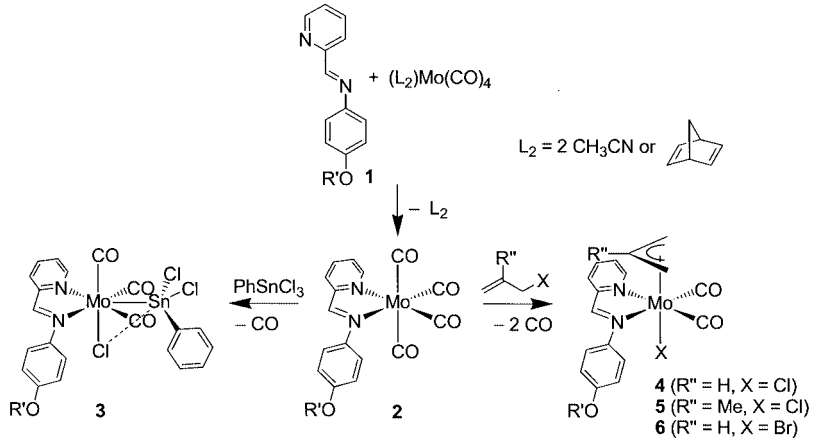

Scheme 2. Solid-phase and solution syntheses of **3**−**6** [a: R′ = H; b: R′ = polystyrene−Si(*i*Pr)$_2$]

The synthesis of Mo^{II} complexes from Mo^0 complexes on the solid phase and in solution is depicted in Scheme 2. The tetracarbonyl complexes **2a** and **2b** were prepared from the soluble ligand **1a** or the immobilised ligand **1b** and an $Mo(CO)_4$ source.[11] Oxidative addition of RX gives the seven-coordinate heterobimetallic complexes **3a** and **3b** with concomitant loss of one equivalent of carbon monoxide (RX = $PhSnCl_3$)[11] and the allyl complexes **4a**−**6a** and **4b**−**6b** [RX = CH_2CHCH_2Cl, $CH_2C(CH_3)CH_2Cl$, CH_2CHCH_2Br] with loss of two equivalents of carbon monoxide.

Release of the immobilised complexes from the solid support is accomplished by fluoridolysis of the silyl ether linker followed by protonation of the anionic complexes with acetic acid (Scheme 3).

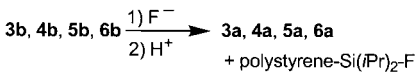

Scheme 3. Cleavage of the complexes from the solid support

All soluble complexes **3a**−**6a** have been completely characterised by spectroscopic methods and the solid-state structures of **3a**−**5a** have been determined by X-ray crystallography. The immobilised complexes **3b**−**6b** have been analysed by IR spectroscopy, diffuse reflection UV/Vis spectroscopy and thermogravimetric analysis.

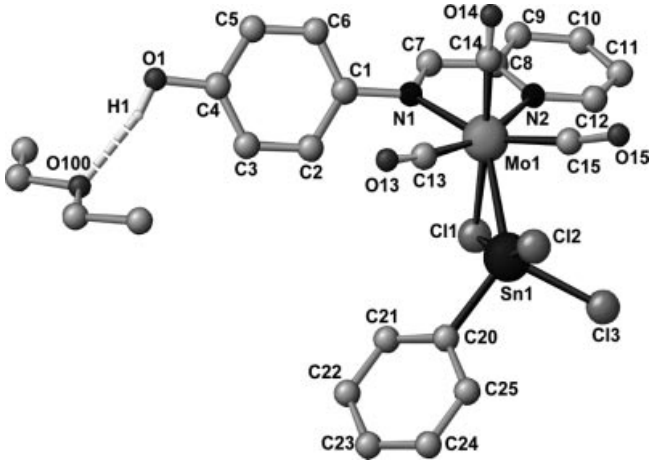

Figure 1. Structure of 3a·Et_2O in the solid state

molybdenum can be described as capped octahedral with the tin atom occupying the seventh position above an octahedral face defined by the bridging chloride Cl1 and two carbon atoms (C13 and C15). The angles between the atoms defining the capped face are larger (104−109°) than the angles between the atoms defining the opposite triangular face (73−96°). Thus, the octahedral symmetry is distorted to accommodate the seventh ligand — similar to the structure of [(bpy)Mo(CO)$_3$Cl(SnCl$_2$CH$_3$)].[21]

Table 1. Selected bond lengths [Å] and angles [°] of **3a**·Et_2O, **4a**·THF, **5a**·THF and **5a**

	3a·Et_2O	**4a**·THF	**5a**·THF	**5a**
Mo1−N1	2.229(2)	2.2732(15)	2.291(2)	2.275(3)
Mo1−N2	2.230(2)	2.2230(16)	2.219(2)	2.247(3)
Mo1−C13	1.982(3)	1.959(2)	1.962(3)	1.958(5)
Mo1−C14	1.976(3)	1.970(2)	1.967(3)	1.955(5)
Mo1−C15	1.983(3)	–	–	–
Mo1−Cl1	2.5409(10)	2.5073(9)	2.5150(8)	2.5149(12)
Mo1−Sn1	2.7154(7)	–	–	–
Mo1−C16	–	2.322(2)	2.319(3)	2.325(4)
Mo1−C17	–	2.208(2)	2.243(2)	2.248(4)
Mo1−C18	–	2.309(2)	2.315(2)	2.304(4)
N1−Mo1−N2	73.17(8)	73.31(5)	73.33(7)	73.43(12)
N1−Mo1−C13	91.10(10)	170.31(7)	169.31(9)	168.71(15)
N1−Mo1−C14	90.46(10)	106.44(7)	105.91(9)	105.30(15)
N1−Mo1−C15	154.33(10)	–	–	–
N1−Mo1−Cl1	84.67(6)	80.97(4)	81.50(5)	79.54(9)
N1−Mo1−Sn1	136.26(6)	–	–	
N1−Mo1−C16	–	114.18(7)	116.89(9)	117.39(15)
N1−Mo1−C17	–	82.14(7)	85.11(9)	85.55(13)
N1−Mo1−C18	–	81.37(7)	83.41(9)	83.69(15)
N2−Mo1−C13	162.57(10)	100.34(7)	100.69(9)	100.69(16)
N2−Mo1−C14	95.91(11)	168.53(7)	168.21(8)	168.95(15)
N2−Mo1−C15	86.96(10)	–	–	–
N2−Mo1−Cl1	81.99(6)	81.15(4)	80.17(5)	82.62(9)
N2−Mo1−Sn1	126.98(5)	–	–	–
N2−Mo1−C16	–	81.16(7)	82.76(9)	82.58(16)
N2−Mo1−C17	–	86.90(7)	88.09(9)	87.49(14)
N2−Mo1−C18	–	120.51(7)	121.71(8)	120.80(14)
C13−Mo1−C14	76.34(13)	78.28(8)	78.08(10)	78.57(18)
C13−Mo1−C15	105.69(13)	–	–	–
C13−Mo1−Cl1	104.43(9)	90.91(6)	88.81(8)	90.24(12)
C13−Mo1−Sn1	69.74(8)	–	–	–
C13−Mo1−C16	–	71.19(9)	70.19(10)	70.45(17)
C13−Mo1−C17	–	105.12(8)	103.76(10)	104.04(16)
C13−Mo1−C18	–	108.29(8)	107.26(10)	107.57(18)
C14−Mo1−C15	75.30(12)	–	–	–
C14−Mo1−Cl1	175.07(8)	87.48(6)	88.07(7)	86.35(12)
C14−Mo1−Sn1	120.32(8)	–	–	–
C14−Mo1−C16	–	108.80(8)	107.50(10)	107.27(18)
C14−Mo1−C17	–	104.49(8)	103.62(10)	103.42(17)
C14−Mo1−C18	–	70.30(8)	69.38(9)	69.45(17)
C15−Mo1−Cl1	108.95(8)	–	–	–
C15−Mo1−Sn1	68.94(8)	–	–	–
Cl1−Mo1−Sn1	64.20(2)	–	–	–
C16−Mo1−C17	–	36.16(8)	35.73(10)	35.61(16)
C16−Mo1−C18	–	61.76(9)	61.52(10)	60.95(18)
C17−Mo1−C18	–	36.08(8)	36.32(9)	35.96(16)
C16−C17−C18	–	115.4(2)	114.1(2)	113.6(4)
H1···A	1.92(3)[a]	2.38(3)[b]	2.45(4)[b]	2.37(4)[b]
O1···A	2.738[a]	3.118[b]	3.145[b]	3.121[b]
O1−H1···A	166(4)[a]	176(3)[b]	179(4)[b]	175(4)[b]
C3−C4−O1−H1	1.6	−177.4	−178.7	−1.2
C7−N1−C1-C2	123.4(3)	−146.2(2)	−147.9(2)	−144.3(4)

[a] A = O100. [b] A = Cl1.

The allyl complex **4a** crystallises in the monoclinic space group $P2_1/c$ with inclusion of one THF molecule. Unlike the structure of **3a** the solvent molecule is isolated from the molybdenum complex. Instead, the hydroxy group of the ligand forms a hydrogen bond to the chloro ligand of a neighbouring molecule (Figure 2). The molecules are thus connected by O−H···Cl hydrogen bonds (O1···Cl1 3.12 Å) and form a chain consisting of alternating enantiomeric complexes along the *c*-axis (*c* glide plane).

The methallyl complex **5a** can be crystallised with and without inclusion of solvent molecules (**5a**·THF and **5a**). In the former pseudo-polymorph the THF molecule is isolated from the complex molecules which are connected by O−H···Cl hydrogen bonds (O1···Cl1 3.15 Å) to give the same motif as the allyl complex **4a** with the chain going along the crystallographic *n* axis. (Figure 3).

The solvent-free pseudo-polymorph of **5a** also displays an O−H···Cl hydrogen bonding motif (O1···Cl1 3.12 Å, Figure 4). Here the complexes form a helix along the crystallographic twofold axis and thus the helices consist of molecules with like stereochemistry (homochiral chain). A further difference is observed for the orientation of the OH group of the ligand in the pseudo-polymorphs **5a**·THF and **5a**: in the former structure the OH bond points away from the metal centre (torsion angle C3−C4−O1−H1 −178.7°, Figure 3) and in the latter it points towards the metal centre (torsion angle C3−C4−O1−H1 −1.2°, Figure 4) as a consequence of the arrangement of the molecules. Obviously the mere presence (**4a**·THF, **5a**·THF) or absence of solvent molecules (**5a**) controls the hetero- or homochirality of the chains without affecting the mode of connection. The O−H···Cl hydrogen bond indeed appears to be the most stable one in this system as no hydrogen bonds between the OH group and solvent molecules {as found for example for **3a** or [(**1a**)$Mo(CO)_3(PPh_3)$]·Et_2O[20]} or metal-bound carbonyl groups [as found for example in complexes {[(**1a**)$M(CO)_3(CNR)$];[20,22] M = Cr, Mo, W} are observed. DFT calculations for **4a** and **5a** with a water molecule (as a model hydrogen donor) hydrogen-bonded to chloride, to the carbonyl ligands, and to the hydroxo group show that the first hydrogen-bonded system is the most stable (although the calculated relative energies might not be be very accurate due to the basis set superposition error BSSE,[23] see Supporting Information).

Properties of 3a, 4a, 5a and 6a

The hydrogen bonding present in the solid-state structures of **3a**, **4a** and **5a** is also confirmed by the signals of the ν_{OH} vibrations at 3444, 3265 and 3256 cm^{-1} in the IR spectra. For the bromo derivative **6a** this band is found at 3173 cm^{-1} which also indicates a hydrogen-bonded structure in the solid state.

Complex **3a** shows three ν_{CO} absorption bands both in solution (Figure 5) and in the solid state, at similar energies, proving that only one isomer is present in solution which most likely has the same geometry as in the solid state (Figure 1).

The signals of the symmetric and asymmetric carbonyl stretching vibrations of the allyl complexes **4a**−**6a** are found at around 1950 and 1874 cm^{-1} (Table 2) at similar energies to the signals of complexes with phenanthroline ligands where the bidentate ligand occupies two equatorial positions, but at considerably higher energies than the sig-

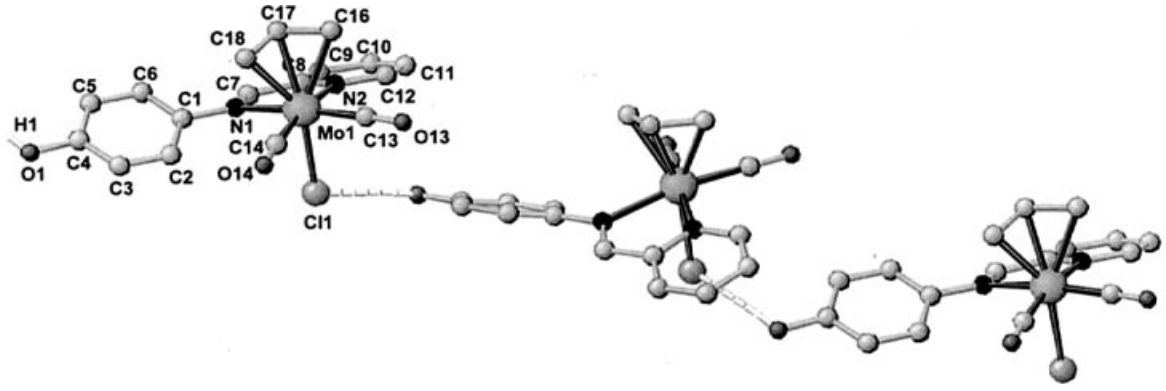

Figure 2. Structure of **4a**·THF in the solid state

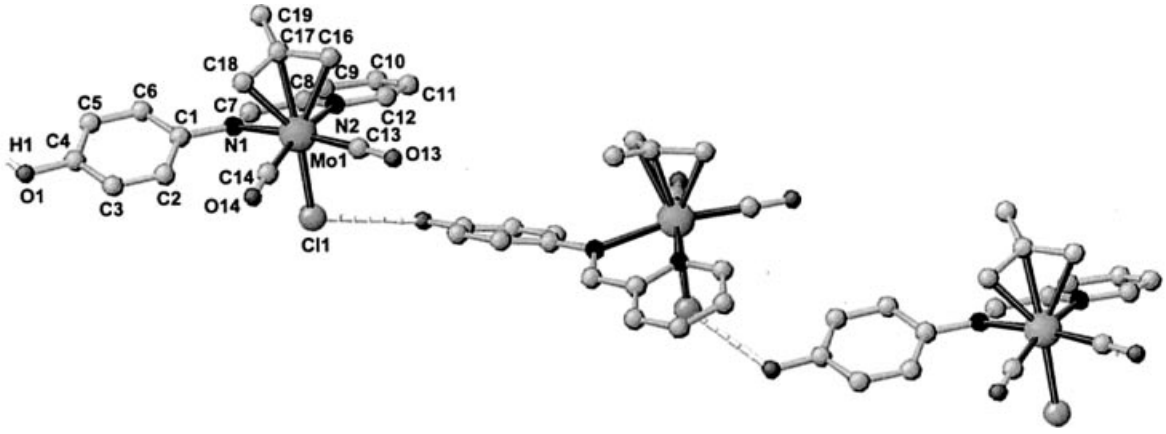

Figure 3. Structure of **5a**·THF in the solid state

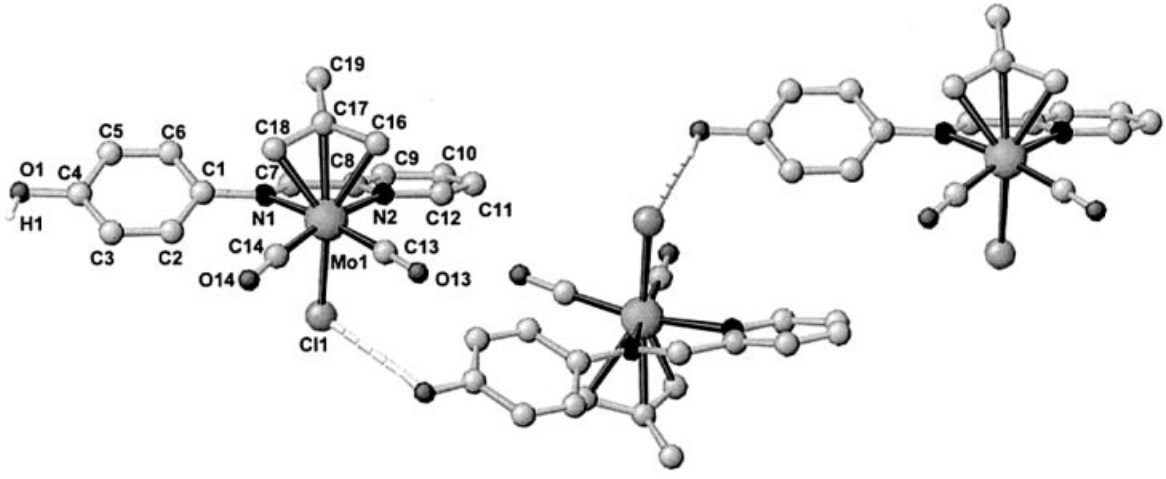

Figure 4. Structure of **5a** in the solid state

nals of complexes where the bidentate ligand occupies one equatorial and one axial position.[24] Thus the IR data suggest that **1a** exclusively coordinates at two equatorial positions in **4a**−**6a** in solution.[24,25]

For the allyl complexes **4a**−**6a** the symmetric and asymmetric carbonyl stretching vibrations are shifted slightly to lower energy in the solid state than in solution (Table 2; $\Delta\tilde{\nu}_{sym/asym}$ = 3/6, 7/11 and 14/11 cm^{-1} for **4a**, **5a** and **6a**). The same shift is predicted by DFT calculations on **4a** and **5a** upon addition of a water molecule hydrogen bonded to the chloro ligand — $\Delta\tilde{\nu}_{sym/asym}$ = 5/9 and 5/10 cm^{-1} for **4a** and **5a**, respectively — explaining the shift by the hydrogen bond to the rather remote chloro ligand. For hydrogen bonds to metal-coordinated carbonyl groups larger shifts are observed experimentally and predicted theoretically[20,22] (for water attached to carbonyl groups of **4a** and **5a** $\Delta\tilde{\nu}_{sym/asym}$ = 9−10/30−36 cm^{-1} are calculated, see Supporting Information).

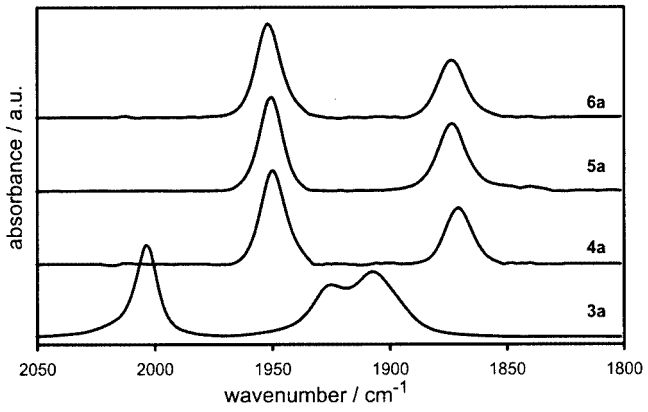

Figure 5. IR spectra of **3a**−**6a** in THF

Table 2. Characteristic IR absorptions of **3a**−**6a**

	$\tilde{\nu}_{CO}$ (cm^{-1})[a]	$\tilde{\nu}_{CO}$ (cm^{-1})[b]	$\tilde{\nu}_{OH}$ (cm^{-1})[b]
3a	2003, 1925, 1907[c]	2009, 1926, 1905[c]	3444
4a	1950, 1871[d]	1947, 1865[d]	3265
5a	1951, 1874[d]	1944, 1863[d]	3256
6a	1952, 1874[d]	1938, 1863[d]	3173

[a] In THF. [b] In CsI. [c] Totally symmetric vibration of all three CO ligands, symmetric vibration of the equatorial CO ligands, asymmetric vibration of the equatorial CO ligands, respectively. [d] Symmetric vibration of the equatorial CO ligands, asymmetric vibration of the equatorial CO ligands, respectively.

In the UV/Vis spectra all complexes display π-π* transitions of the Schiff-base ligand at around 356 nm (Figure 6, Table 3). The seven-coordinate complex **3a** has an MLCT absorption band at λ = 474 nm and is irreversibly reduced at E = −850 mV (Table 3). The allyl complexes **4a**−**6a** show MLCT absorption bands between 500 and 620 nm (Figure 6). The allyl and halide ligands influence the energy of the MLCT absorption according to their electron-donating and -withdrawing properties. The same consideration applies for the potentials of the metal-centred oxidations, as **5a** and **6a** are easier to oxidise than **4a**.

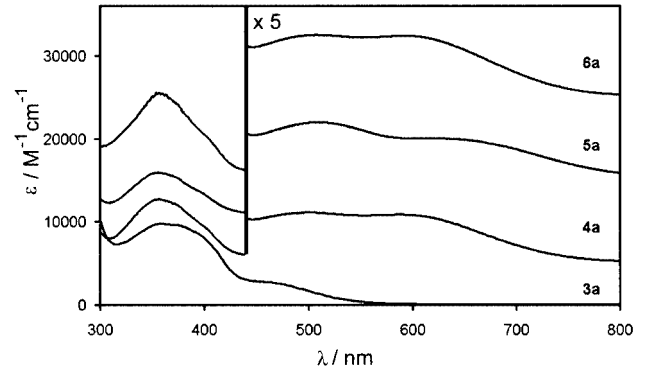

Figure 6. UV/Vis spectra of **3a**−**6a**

The solution structures of the complexes **4a**−**6a**, i.e. the orientations of the allyl ligands with respect to the Schiff-base ligands, have been determined by ^{1}H and ^{13}C NMR spectroscopy (Table 4 and 5). In the ^{1}H NMR spectra the allyl complexes **4a** and **6a** display an ABCDX pattern for the signals of the allyl ligand and **5a** shows an ABCD pattern, both of which suggest static structures in solution (e.g. absence of η^3-η^1-η^3 rearrangements of the allyl ligands). In the NOESY spectra, in addition to cross-peaks between intraligand protons (allyl and Schiff-base ligand), cross-peaks between allyl protons and Schiff-base ligand protons are observed (Figure 7). These observations show that the η^3-allyl ligands are oriented with the open face towards the carbonyls, which is the same orientation as found in the solid state for **4a** and **5a**. This is substantiated by the similar solution and solid state IR spectra of **4a**, **5a** and **6a** (Table 2).

Polymer-Bound Complexes 3b−6b

All polymer-bound complexes were characterised by IR and diffuse reflection UV/Vis spectroscopy and thermogravimetric analysis (Table 6).[11,12]

The IR spectra of the immobilised complexes **3b**−**6b** are shown in Figure 8. In addition to the intense signals of vibrations of the polymer backbone, signals in the characteristic ν_{CO} region are observed. These data compare well with those for the soluble complexes **3a**−**6a** (Table 2 and 6) confirming the presence of immobilised carbonyl complexes with the same stereochemistry as found in the solid state and in solution.

The UV/Vis absorption maxima of resins **3b**−**6b** (Figure 9) are shifted to lower energy than their solution counterparts (Table 3 and 6) but the trend of the MLCT transitions λ_{max}(**3**) << λ_{max}(**4**) < λ_{max}(**6**) < λ_{max}(**5**) is the same for the soluble and polymer-bound complexes. A similar behaviour has been observed for soluble and immobilised Mo^0 complexes.[11,12]

The thermal stability of **3b**−**6b** has been investigated by thermogravimetric analysis. For **3b** a larger weight loss of

Table 3. UV/Vis spectroscopic and cyclovoltammetric data of **3a**−**6a**

	λ_{max}/nm (ε/M^{-1} cm^{-1})			$E_{1/2}$/mV (ΔE/mV)[a]
3a	358 (9755)[b]	474 (2515)[b]		−850 mV (irr.; reverse scan: +40 mV)
4a	354 (7710)[c]	501 (1220)[c]	590 (1175)[c]	610 (100)
5a	356 (5920)[c]	510 (1400)[c]	620 (1010)[c]	515 (110)
6a	357 (10600)[c]	507 (1500)[c]	594 (1480)[c]	605 (90)

[a] 10^{-3} M in 0.1 M (nBu$_4$N)PF$_6$/CH$_2$Cl$_2$, vs. SCE. [b] In CH$_2$Cl$_2$. [c] In THF.

Table 4. ^{1}H NMR spectroscopic data of **3a**−**6a**

	3a[a]	**4a**[b]	**5a**[b]	**6a**[b]
Ph	7.38 (m), 8.00 (m)	–	–	–
H[a]	–	2.5[c]	2.20 (d, J = 3.2 Hz)	2.5[c]
H^b	–	1.00 (d, J = 8.7 Hz)	1.04 (s)	1.04 (d, J = 8.0 Hz)
H^c	–	1.22 (d, J = 8.7 Hz)	1.22 (s)	1.28 (d, J = 8.0 Hz)
H^d	–	3.14 (bs)	2.84 (d, J = 3.2 Hz)	3.15 (bs)
R	–	3.3−3.4 (m)[d]	1.30 (s)[e]	3.37 (bs)[d]
H^{3,5}	6.87 (d, J = 8.4 Hz)	6.90 (d, J = 7.9 Hz)	6.91 (d, J = 8.4 Hz)	6.90 (d, J = 8.0 Hz)
H^{2,6}	7.41 (d, J = 8.4 Hz)	7.47 (d, J = 7.9 Hz)	7.32 (d, J = 8.4 Hz)	7.51 (d, J = 8.0 Hz)
H^{11}	7.78 (pt)	7.71 (bs)	7.68−7.75 (m)	7.70 (bs)
H$^{9/H10}$	8.09 (d, J = 7.2 Hz), 8.21 (pt)	8.1−8.2 (m)	8.2−8.3 (m)	8.2−8.3 (m)
H^{12}	9.10 (d, J = 4.8 Hz)	8.82 (d, J = 3.8 Hz)	8.79 (d, J = 5.4 Hz)	8.82 (d, J = 4.0 Hz)
H^7	8.64 (s)	8.71 (s)	8.82 (s)	8.71 (s)
OH	8.87 (s)	9.90 (s)	9.93 (s)	9.89 (s)

[a] In [D$_8$]THF. [b] In [D$_6$]DMSO. [c] Under solvent signal. [d] H^{17}. [e] H^{19}.

Table 5. ^{13}C NMR spectroscopic data of **3a**−**6a**

	3a[a]	**4a**[b]	**5a**[b]	**6a**[b]
Ph	143.8,[c] 129.2,[d] 130.6,[e] 136.2[f]	–	–	–
C^{16}	–	56.6	54.2	55.6
C^{17}	–	74.2	82.9	74.7
C^{18}	–	53.8	52.7	53.1
C^{19}	–	–	19.6	–
C^1	149.8	142.8	142.7	143.0
C^{2,6}	124.4	124.3	124.5	124.4
C^{3,5}	116.7	116.3	116.4	116.2
C^4	154.1	153.9	154.0	154.0
C^7	166.6	164.4	164.2	164.3
C^8	157.9	158.8	159.0	158.8
C^9	130.4	129.9	130.2	130.0
C^{10}	141.7	140.0	140.0	139.9
C^{11}	130.0	128.3	128.3	128.2
C^{12}	154.3	152.8	152.5	153.0
CO	215.1/224.9/227.7	227.6/228.2	227.6/228.4	226.8/227.4

[a] In [D$_8$]THF. [b] In [D$_6$]DMSO. [c] C-*ipso*. [d] C-*ortho*, $^2J_{Sn,C}$ = 87 Hz. [e] C-*para*, $^4J_{Sn,C}$ = 18 Hz. [f] C-*meta*, $^3J_{Sn,C}$ = 61 Hz.

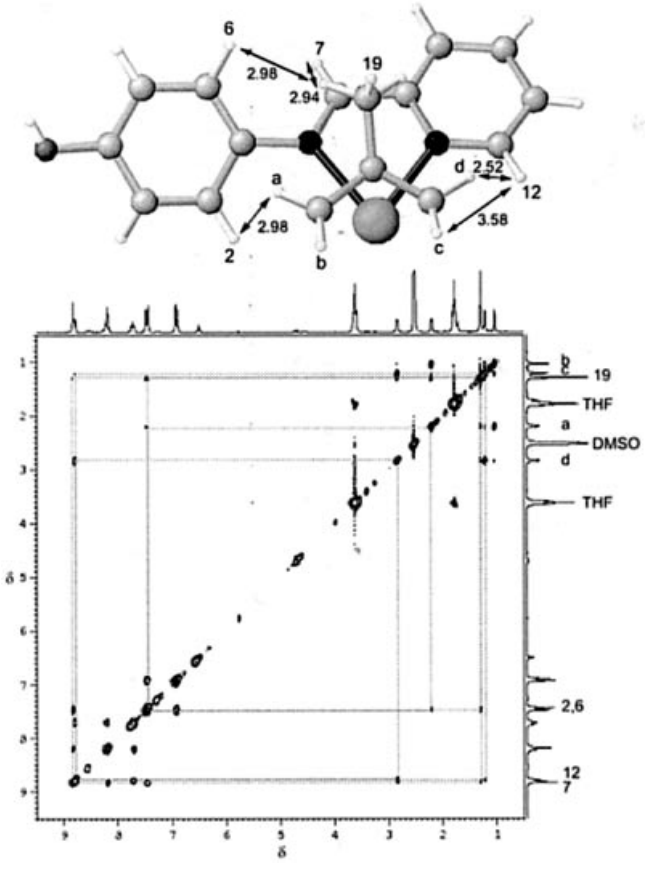

Figure 7. Relevant NOE contacts and distances [Å] (solid-state structure) between protons of the allyl ligand and the Schiff-base ligand in complex **5a** (top); NOESY spectrum of **5a**·THF in [D$_6$]DMSO (bottom)

6.1% is observed at 200 °C, which can be accounted for by a loss of three carbon monoxide ligands and one chloro ligand, while the immobilised allyl complexes **4b**−**6b** only lose coordinated carbonyl ligands up to 200 °C (Table 6). Carbon monoxide loss has also been detected for immobilised Mo^0 carbonyl complexes.[12] These data show that these complexes are formed quantitatively on the solid support and that allyl complexes are thermally more stable than the seven-coordinate molybdenum-tin complex.

Treating the resins **3b**−**6b** with tetra-*n*-butylammonium fluoride in dichloromethane (Scheme 3) results in deeply coloured solutions of the deprotonated complexes **3a**$^-$−**6a**$^-$ which were characterised by IR spectroscopy (Table 7). The signals of the ν_{CO} vibrations of **3a**$^-$−**6a**$^-$ are shifted to lower energy relative to the signals of the neutral parent complexes **3a**−**6a** (Table 2), as expected.

After washing the resins and concentrating the filtrates careful acidification with acetic acid yields solutions of the complexes **3a**−**6a**. In all cases no spectroscopic evidence was observed for the formation of side products, confirming the identity and stability of the polymer-bound complexes.

Table 6. Analytical data of polymer-bound complexes **3b**−**6b**

	ν_{CO} (cm^{-1})	λ_{max} (nm)	$\Delta m/m$ (exp.) (%)[a]	$\Delta m/m$ (calcd.) (%)[b]
3b	2008, 1930, 1912	449, 533 (sh)	6.1	6.03
4b	1953, 1871	460 (sh), 673	3.2	3.24
5b	1953, 1878	460 (sh), 708, 810 (sh)	3.1	3.21
6b	1952, 1872	460 (sh), 699	3.1	3.16

[a] At 200°C. [b] The theoretical amount of weight loss is calculated according to the following formula: $\Delta m/m = 100 * (n_{CO} * M_{CO} + n_{Cl} * M_{Cl})/(M_{resin} + M_{complex\ fragment})$ with $n_{CO} = 3$ and $n_{Cl} = 1$ (**3b**), $n_{CO} = 2$ and $n_{Cl} = 0$ (**4b**, **5b**, **6b**), $M_{CO} = 28$ g mol^{-1}, $M_{Cl} = 35.5$ g mol^{-1}, $M_{resin} = 1500$ g mol^{-1} (resin loading 0.5 mmol g^{-1}), $M_{complex\ fragment} = 482.1$ [**3b**: $PhSnCl_3Mo(CO)_3$], 228.5 [**4b**: $C_3H_5ClMo(CO)_2$], 242.5 [**5b**: $C_4H_7ClMo(CO)_2$] and 272.9 [**6b**: $C_3H_5BrMo(CO)_2$] g mol^{-1} giving $\Delta m/m = 6.03$, 3.24 , 3.21 and 3.16%, respectively.

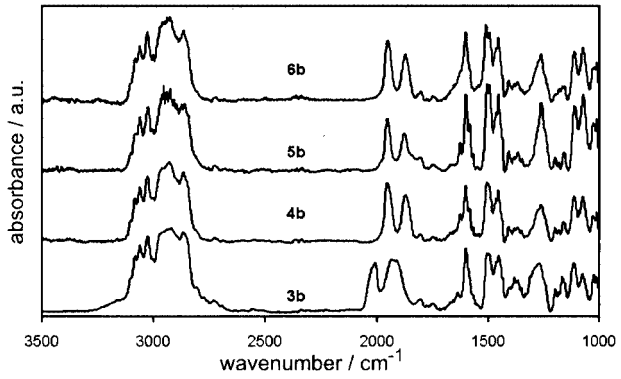

Figure 8. IR spectra of resins **3b**−**6b**

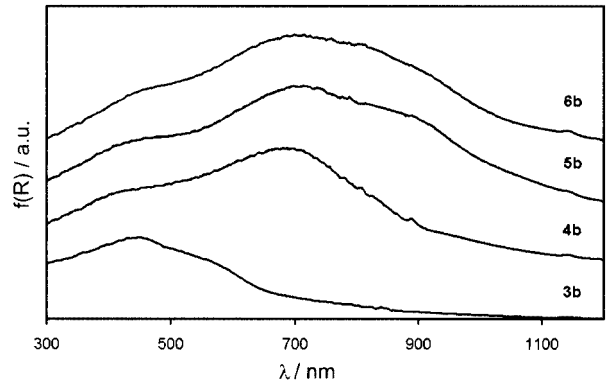

Figure 9. Diffuse reflection UV/Vis spectra of resins **3b**−**6b**

Table 7. Characteristic IR absorptions of **3a**$^-$−**6a**$^-$ in THF

	ν_{CO} (cm^{-1})
3a	1992, 1915, 1895[a]
4a	1943, 1861[b]
5a	1945, 1864[b]
6a	1946, 1864[b]

[a] Totally symmetric vibration of all three CO ligands, symmetric vibration of the equatorial CO ligands, asymmetric vibration of the equatorial CO ligands, respectively. [b] Symmetric vibration of the equatorial CO ligands, asymmetric vibration of the equatorial CO ligands, respectively.

Conclusion

Oxidative addition of RX ($PhSnCl_3$ or allyl halides) to the molybdenum tetracarbonyl complexes **2a**/**2b** furnishes the molybdenum(II) complexes **3a**−**6a**/**3b**−**6b**.

The stereochemistry of the complexes has been elucidated by single-crystal X-ray diffraction in the solid state and by NMR and IR spectroscopy in solution. The bimetallic molybdenum-tin complex **3a** has a capped octahedral coordination geometry with the tin occupying the seventh position above an octahedral face. The allyl complexes **4a**−**6a** have an octahedral coordination geometry with the bidentate Schiff-base ligand occupying two equatorial positions and the η^3-allyl ligand oriented with the open face towards the carbonyl ligands.

The reactions with polymer-bound complexes proceed quantitatively, as shown by IR spectroscopy and thermogravimetric analysis. The stereochemistry of the polymer-bound complexes **3b**−**6b** is the same as for the soluble complexes **3a**−**6a** in solution and in the solid state. The stability and identity of polymer-bound complexes has been demonstrated by release of the complexes from the polymer. These results pave the way for the immobilisation of active and selective molybdenum catalysts for (enantioselective) allylic alkylation reactions on polymeric supports.

Experimental Section

Unless noted otherwise, all manipulations were carried out under argon by means of standard Schlenk techniques. All solvents were dried by standard methods and distilled under argon prior to use. Complexes **1a**−**3a** and **1b**−**3b** were prepared by a literature method.[11,12] All other reagents were used as received from commercial sources.

NMR: Bruker Avance DPX 200 at 200.15 MHz (^1H), 50.323 MHz (^{13}C) at 303 K; chemical shifts (δ) in ppm with respect to residual solvent peaks as internal standards: $[D_6]DMSO$ (^1H: δ = 2.49 ppm; ^{13}C: δ = 39.7 ppm), $[D_8]THF$ (^1H: δ = 1.73, 3.58 ppm; ^{13}C: δ = 25.5, 67.7 ppm). IR spectra were recorded on a BioRad Excalibur FTS 3000 spectrometer using CaF_2 cells or CsI disks. UV/Vis/NIR spectra were recorded on a Perkin−Elmer Lambda 19 instrument with 0.2 cm cells (Hellma, suprasil). DRS-UV/Vis spectra were measured with the same instrument using the Perkin−Elmer inte-

grating sphere and poly(tetrafluoroethylene) as reference. Cyclic voltammetry was performed using a glassy carbon electrode, a platinum electrode and an SCE electrode, 10^{-3} M in 0.1 M nBu$_4$NPF$_6$/CH$_2$Cl$_2$, potentials are given relative to that of SCE. Mass spectra were recorded on a Finnigan MAT 8400 spectrometer with a matrix of 4-nitrobenzyl alcohol (FAB). Elemental analyses were performed by the microanalytical laboratory of the Organic Chemistry Department, University of Heidelberg. Thermogravimetric measurements were carried out on a Mettler TC 15; heating rate: 10 K min^{-1} under argon from 30−800 °C.

Solution Syntheses of 4a−6a: The appropriate 3-halopropene (2 mmol) was added to a solution of **2a** (406 mg, 1 mmol) in THF (30 mL). The solution was heated under reflux until IR spectroscopy indicated disappearance of the bands of **2a** and complete formation of the product (3−4 h). The solvent was removed under reduced pressure and the crude product was washed with diethyl ether and recrystallised from THF/diethyl ether or CH$_2$Cl$_2$/diethyl ether.

4a: Yield: 311 mg, 0.73 mmol (73%). C$_{17}$H$_{15}$ClMoN$_2$O$_3$ (426.71): calcd. C 47.85, H 3.54, N 6.57; found C 48.04, H 3.79, N 6.40. MS (FAB): *m/z* (%) = 428 (100) [M$^+$ + H], 393 (41) [M$^+$ − Cl], 372 (97) [M$^+$ − 2CO].

5a: Yield: 366 mg, 0.83 mmol (83%). C$_{18}$H$_{17}$ClMoN$_2$O$_3$·THF (440.73·THF): calcd. C 51.52, H 4.91, N 5.46; found C 51.32, H 5.20, N 5.86. MS (FAB): *m/z* (%) = 442 (42) [M$^+$ + H], 407 (21) [M$^+$ − Cl], 386 (100) [M$^+$ − 2CO].

6a: Yield: 419 mg, 0.89 mmol (89%). C$_{17}$H$_{15}$BrMoN$_2$O$_3$·0.5THF (471.16·0.5THF): calcd. C 44.99, H 3.78, N 5.52; found C 45.18, H 4.02, N 5.27. MS (FAB): *m/z* (%) = 472 (12) [M$^+$ + H], 393 (100) [M$^+$ − Br], 416 (23) [M$^+$ − 2CO].

Solid-Phase Synthesis of 4b−6b: The appropriate 3-halopropene (1 mmol) was added to a suspension of **2b** (500 mg, 0.25 mmol) in THF (30 mL). The suspension was heated under reflux until IR spectroscopy of a polymer sample indicated formation of the product and complete conversion of the starting complex (8−10 h). The dark polymer was isolated by filtration, washed with THF and diethyl ether and dried in vacuo.

Cleavage procedure: A solution of tetra-*n*-butylammonium fluoride TBAF·3H$_2$O (2 equivalents) in THF was added to a suspension of the appropriate resin in THF (10 mL). The suspension was stirred for 6 h at room temperature. IR spectroscopy of the solution indicated release of the anionic complexes **4a**$^-$**−6a**$^-$. The mixture was filtered and the polymer was washed with THF until the solution was colourless. The combined filtrates were acidified with acetic acid giving **4a−6a** in 60%, 52% and 71% yield, respectively, based on the loading of **1b**. After cleavage, mass spectrometry of the remaining silyl fluoride polymer indicated complete removal of the complexes.[10]

Computational Methods: Density functional calculations were carried out with the Gaussian98/DFT[26] program series. The B3LYP formulation of density functional theory was used employing the LanL2DZ basis set.[26] Harmonic vibrational frequencies and infrared intensities were calculated by numerical second derivatives using analytically calculated first derivatives. Frequencies are not scaled.

Crystallographic Structure Determinations: The measurements were carried out on an Enraf−Nonius Kappa CCD diffractometer using graphite monochromated Mo-K_α radiation. The data were processed using the standard Nonius software.[27] All calculations were performed using the SHELXT PLUS software package. Structures were solved using direct or Patterson methods with the SHELXS-97 program and refined with the SHELXL-97 program.[28] Graphical handling of the structural data during refinement was performed using XMPA[29] and WinRay.[30] Atomic coordinates and anisotropic thermal parameters of the non-hydrogen atoms were refined by full-matrix least-squares calculations. Data relating to the structure determinations are collected in Table 8.

Table 8. X-ray crystallographic data of complexes **3a**·Et$_2$O, **4a**·THF, **5a**·THF and **5a**.

	3a·Et$_2$O	**4a**·THF	**5a**·THF	**5a**
Formula	C$_{25}$H$_{25}$Cl$_3$N$_2$O$_5$SnMo	C$_{21}$H$_{23}$ClN$_2$O$_4$Mo	C$_{22}$H$_{25}$ClN$_2$O$_4$Mo	C$_{18}$H$_{17}$ClN$_2$O$_3$Mo
Molecular mass	754.45	498.80	512.83	440.73
Crystal dimension/mm	0.20 × 0.10 × 0.10	1.00 × 0.50 × 0.25	0.30 × 0.30 × 0.20	0.25 × 0.10 × 0.10
Crystal system	monoclinic	monoclinic	monoclinic	monoclinic
Space group (no.)	$P2_1/c$ (14)	$P2_1/c$ (14)	$P2_1/n$ (14)	$P2_1/n$ (14)
a (Å)	7.6940(15)	10.568(2)	13.128(3)	8.939(2)
b (Å)	31.704(6)	10.403(2)	10.566(2)	16.163(3)
c (Å)	12.171(2)	19.905(4)	15.603(3)	12.729(3)
β (°)	101.09(3)	103.32(3)	91.73(3)	103.45(3)
Cell volume (Å^3)	2913.4(10)	2137.9(7)	2163.3(7)	1788.3(6)
Molecular units per cell	4	4	4	4
μ (mm^{-1})	1.599	0.768	0.761	0.902
Density (calcd.) (g cm^{-3})	1.720	1.550	1.575	1.637
T (K)	200	200	200	200
Scan range (2Θ)	3.6−60.1	3.9−30.1	4.0−61.1	4.1−55.0
Scan speed (sec frame^{-1})	10	8	6	30
Measured reflections	16483	14311	11494	6728
Unique reflections	8499	6158	6206	3971
Obs. reflections ($I \geq 2\sigma$)	5933	4945	5096	2670
Parameters refined	398	354	371	294
Max. resid. elec. density (e·Å^{-3})	0.64/−0.72	0.71/−0.67	1.10/−0.95	0.72/−0.57
Agreement factors	R_1 = 3.9%	R_1 = 3.1%	R_1 = 4.5%	R_1 = 4.7%
(F^2 refinement)	R_w = 7.8%	R_w = 7.7%	R_w = 12.0%	R_w = 11.4%

CCDC-225156−225159 (**3a**·Et_2O, **4a**·THF, **5a**·THF and **5a**) contains the supplementary crystallographic data for this paper. These data can be obtained free of charge at www.ccdc.cam.ac.uk/conts/retrieving.html [or from the Cambridge Crystallographic Data Centre, 12 Union Road, Cambridge CB2 1EZ, UK; Fax: (internat.) +44-1223/336-033; E-mail: deposit@ccdc.cam.ac.uk].

Acknowledgments

This work was supported by the Deutsche Forschungsgemeinschaft and the Fonds der Chemischen Industrie. The permanent, generous support from Prof. Dr. G. Huttner is gratefully acknowledged. We thank Michela Doria for preparative assistance.

[1] *Chiral Catalyst Immobilisation and Recycling* (Eds.: E. De Vos, I. F. J. Vankelecom, P. A. Jacobs), **2000**, Wiley-VCH, Weinheim.
[2] S. Bräse, D. Enders, J. Köbberling, F. Avemaria, *Angew. Chem.* **1998**, *110*, 3614−3614; *Angew. Chem. Int. Ed.* **1998**, *37*, 3413−3415.
[3] R. Zanaletti, M. Freccero, *Chem. Commun.* **2002**, 1908−1909.
[4] S. Dahmen, S. Bräse, *Angew. Chem.* **2000**, *112*, 3827−3830; *Angew. Chem. Int. Ed.* **2000**, *39*, 3681−3683.
[5] P. Hodge, *Chem. Soc. Rev.* **1997**, *26*, 417−424.
[6] B. Pugin, *J. Mol. Catal. A* **1996**, *107*, 273−279.
[7] R. Grubbs, C. P. Lau, R. Cukier, C. Brubaker Jr., *J. Am. Chem. Soc.* **1977**, *99*, 4517−4518.
[8] X.-W. Yang, J.-H. Sheng, C.-S. Da, H.-S. Wang, W. Su, R. Wang, A. S. C. Chan, *J. Org. Chem.* **2000**, *65*, 295−296.
[9] B. Altava, M. I. Burguete, J. M. Fraile, J. I. García, S. V. Luis, J. A. Mayoral, M. J. Vicent, *Angew. Chem.* **2000**, *112*, 1563−1566; *Angew. Chem. Int. Ed.* **2000**, *39*, 1503−1506.
[10] K. Heinze, U. Winterhalter, T. Jannack, *Chem. Eur. J.* **2000**, *6*, 4203−4210.
[11] K. Heinze, *Chem. Eur. J.* **2001**, *7*, 2922−2932.
[12] K. Heinze, J. B. Toro, *Angew. Chem.* **2003**, *115*, 4671−4674; *Angew. Chem. Int. Ed.* **2003**, *42*, 4533−4536.
[13] B. M. Trost, I. Hachiya, *J. Am. Chem. Soc.* **1998**, *120*, 1104−1105.
[14] B. M. Trost, S. Hildbrand, K. Dogra, *J. Am. Chem. Soc.* **1999**, *121*, 10416−10417.
[15] F. Glorius, A. Pfaltz, *Org. Lett.* **1999**, *1*, 141−144.
[16] M. Palucki, J. M. Um, D. A. Conlon, N. Yusada, D. L. Hughes, B. Mao, J. Wang, P. J. Reider, *Adv. Synth. Catal.* **2001**, *343*, 46−50.
[17] N.-F. K. Kaiser, U. Bremberg, M. Larhed, C. Moberg, A. Hallberg, *Angew. Chem.* **2000**, *112*, 3742−3744; *Angew. Chem. Int. Ed.* **2000**, *39*, 3595−3598.
[18] Y. Uozumi, H. Danjo, T. Hayashi, *Tetrahedron Lett.* **1997**, *38*, 3557−3560.
[19] D. R. van Staveren, N. Metzler-Nolte, *Chem. Commun.* **2002**, 1406−1407.
[20] K. Heinze, *J. Chem. Soc., Dalton Trans.* **2002**, 540−547.
[21] M. Elder, D. Hall, *Inorg. Chem.* **1969**, *8*, 1268−1273.
[22] K. Heinze, V. Jacob, *J. Chem. Soc., Dalton Trans.* **2002**, 2379−2385.
[23] W. Koch, M. C. Holthausen, *A Chemist's Guide to Density Functional Theory*, Wiley-VCH, Weinheim, **2001**.
[24] M. P. T. Sjögren, H. Frisell, B. Åkermark, *Organometallics* **1997**, *16*, 942−950.
[25] P. Espinet, R. Hernando, G. Iturbe, F. Villafañe, G. A. Orpen, I. Pascual, *Eur. J. Inorg. Chem.* **2000**, 1031−1038.
[26] M. J. Frisch, G. W. Trucks, H. B. Schlegel, G. E. Scuseria, M. A. Robb, J. R. Cheeseman, V. G. Zakrzewski, J. A. Montgomery, Jr., R. E. Stratmann, J. C. Burant, S. Dapprich, J. M. Millam, A. D. Daniels, K. N. Kudin, M. C. Strain, O. Farkas, J. Tomasi, V. Barone, M. Cossi, R. Cammi, B. Mennucci, C. Pomelli, C. Adamo, S. Clifford, J. Ochterski, G. A. Petersson, P. Y. Ayala, Q. Cui, K. Morokuma, D. K. Malick, A. D. Rabuck, K. Raghavachari, J. B. Foresman, J. Cioslowski, J. V. Ortiz, B. B. Stefanov, G. Liu, A. Liashenko, P. Piskorz, I. Komaromi, R. Gomperts, R. L. Martin, D. J. Fox, T. Keith, M. A. Al-Laham, C. Y. Peng, A. Nanayakkara, C. Gonzalez, M. Challacombe, P. M. W. Gill, B. Johnson, W. Chen, M. W. Wong, J. L. Andres, C. Gonzalez, M. Head-Gordon, E. S. Replogle, J. A. Pople, *Gaussian 98, Revision A.6*, Gaussian, Inc., Pittsburgh PA, **1998**; http://www.gaussian.com.
[27] R. Hooft, Collect, Data Collection Software, Nonius, The Netherlands, **1998**; http://www.nonius.com.
[28] G. M. Sheldrick, *SHELXS-97, Program for Crystal Structure Solution*, University of Göttingen, Germany, **1997**; http://www.shelx.uni-ac.gwdg.de/shelx/index.html; G. M. Sheldrick, *SHELXL-97, Program for Crystal Structure Refinement*, University of Göttingen, Germany, **1997**; http://www.shelx.uni-ac.gwdg.de/shelx/index.html; *International Tables for X-ray Crystallography*, Kynoch Press, Birmingham, U. K., **1974**, vol. 4.
[29] L. Zsolnai, G. Huttner, *XPMA*, University of Heidelberg, Germany, **1998**; http://www.rzuser.uni-heidelberg.de/~il1/laszlo/xpm.html.
[30] R. Soltek, G. Huttner, *WinRay*, University of Heidelberg, Germany, **1999**; http://www.uni-heidelberg.de/institute/fak12/AC/huttner/frame/frame_soft.html.

Received December 5, 2003
Early View Article
Published Online April 1, 2004

